Proceedings of the 7th International Symposium on Cavitation
CAV2009
August 17-22, 2009, Ann Arbor, Michigan, USA

CAV2009-Paper No. 173

NUMERICAL STUDY ON THE SURFACE STABILITY OF AN ENCAPSULATED MICROBUBBLE IN THE ULTRASOUND FIELD

Yunqiao Liu*
Department of Mechanical Engineering
The University of Tokyo
7-3-1 Hongo, Bunkyo-ku, 113-8656, Tokyo, Japan
Email: yqliu@fel.t.u-tokyo.ac.jp

Kazuyasu Sugiyama
Department of Mechanical Engineering
The University of Tokyo
7-3-1 Hongo, Bunkyo-ku, 113-8656, Tokyo, Japan

Shu Takagi
Organ and Body Scale Team, RIKEN
2-1 Hirosawa, Wako 351-0198, Saitama, Japan
Also at: Department of Mechanical Engineering,
The University of Tokyo

Yoichiro Matsumoto
Department of Mechanical Engineering
The University of Tokyo
7-3-1 Hongo, Bunkyo-ku, 113-8656, Tokyo, Japan

ABSTRACT

The surface stability problem of an encapsulated microbubble in an ultrasound field is numerically addressed. To predict the nonlinear process, the continuity equation and Navier-Stokes equation are directly solved by means of a boundary-fitted finite-volume method on an orthogonal curvilinear coordinate system. The bubble is insonified by an ultrasound pulse consisting of a burst of 10 cycles, of which the first and last two periods are modified by a Gaussian envelope. The simulation code reproduces a shape oscillation of a gas bubble with an initial radius of 30μm at a pressure frequency of 130kHz as shown in experimental and theoretical studies [1]. The effects of the membrane on the shape oscillation are investigated through simulations of a micrometer-sized bubble encapsulated with a neo-Hookean membrane at an ultrasonic frequency of 1MHz. The encapsulated bubble presents a second-order shape instability, while the gas bubble of the same size keeps spherical because the surface tension significantly suppresses the shape oscillation. The strain-softening features with increasing the oscillation amplitude are characterized by a larger expansion and the higher harmonics when the bubble contracts.

NOMENCLATURE

- a amplitude of shape mode
- e rate of strain
- E_b bending modulus
- f frequency of driving acoustic pressure
- F membrane force
- g acceleration of gravity
- G_s surface shear elastic modulus
- h metric coefficients
- K bending strain
- m bending moment
- p pressure
- q transverse shear tension
- r radius of bubble
- s azimuthal direction
- t time
- T_f period of driving acoustic pressure
- u velocity

*Address all correspondence to this author.

V volume of bubble
γ surface tension
ε amplitude of driving acoustic pressure
η η-direction in computational space
κ curvature
λ rate of extension
μ viscosity
ξ ξ-direction in computational space
ρ density
σ distance from axis of symmetry
τ in-plane tension
υ Poisson's ratio
φ meridional direction

Subscript
0 initial state
l liquid
g gas

Superscript
R reference state

INTRODUCTION

Dynamics of an encapsulated microbubble is practically relevant to medical ultrasound diagnostics and therapeutics. Ultrasound contrast agents (UCA) in traditional medical sonography are gas-filled microbubbles coated with polymeric membrane [2]. Due to the compressibility of gas core, the UCA has a high degree of echogenicity, and thus is able to enhance the ultrasound backscatter and to yield high-quality image. The coating membrane protects the gas core from dissolving and withstands bursting under acoustic energy. Drug delivery system (DDS) is another rapidly developing medical application. The DDS utilizes localized ultrasound energy to rupture the encapsulating membrane and under controlled conditions makes the drug reach the targeted [3]. In the rupture process, inhomogeneity in the interfacial stress resulting from deformation is an important ingredient to be examined, in addition to the homogeneous stress increase due to the radial oscillation. In particular, the shape instability enhances the inhomogeneity at a preferred frequency.

The stability problem of a gas bubble was firstly addressed by Plesset [4] limited to the small disturbances of spherical interface in an incompressible and inviscid liquid. Introduced an infinitesimal distortion in shape, the equation about the pulsation amplitude is reduced to the Mathieu's equation characterizing the parametric instability [5]. This instability occurs when the pulsation amplitude exceeds a threshold value that depends on the bubble radius and the frequency of the driving acoustic field [6]. The shape instability interacting with radial oscillation will lead to a resonant response [7], during which periodic energy exchange between the radial and shape modes takes place [8]. This process has been studied experimentally by Mao et al. [9], and simulated by McDougald et al. [10, 11]. When the bubble is exposed to an ultrasound field, surface modes up to $n = 7$ were experimentally observed and theoretically analyzed by Versluis et al. [1].

Since the membrane, which encapsulates gas or drug, will influence the behavior of the bubble motion, its dynamics has become of great interest in recent years. The shape instability and final destruction of different kinds of UCAs were captured by high-speed imaging systems [12, 13]. The pioneering theoretical studies were made for the spherical motion based on the Rayleigh-Plesset equation with additional terms regarding the internal friction inside the shell and the restoring force accounting for shell stiffness [14], and with viscous damping mechanism [15]. A more comprehensive model considers the membrane as a hyperelastic material, which has a shape-reversible structure [16]. The constitutive laws, which connect the membrane strain with the in-plane stress, are derived from the surface energy function. Three typical hyperelastic constitutive laws were compared by Barthès-Biesel et al. [17] in the context of a capsule's motion in a linear shear flow. Using these constitutive laws, Tsiglifis and Pelekasis [18] investigated the nonlinear radial oscillations of an encapsulated microbubble subject to ultrasound.

In the present study, we investigate the surface stability of the encapsulated microbubble subjected to an ultrasonic pressure wave by means of a direct numerical simulation. The boundary-fitted simulation code, which has been developed for the axisymmetrically deformed motion of an incompressible gas bubble [19, 20], is extended to consider the compressibility of the bubble and to couple with the membrane mechanics [21]. We treat the hyperelastic membrane as the neo-Hookean law. First, we examine the shape oscillation of the gas bubble to validate the numerical computation through comparing with the experimental and theoretical results [1]. Second, we investigate the influence of the membrane on the stability of the shape oscillation and the effect of the amplitude of applied ultrasonic pressure on the nonlinearity in hydrodynamics.

PROBLEM FORMULATION

Here we deal with an axisymmetric system, i.e., we do not consider the azimuthal mode in the fluid flow or the interfacial deflection. We adopt the boundary-fitted finite-volume method on an orthogonal curvilinear coordinate system. The grid and the coordinate system are schematically shown in Fig. 1. All the governing equations and the boundary conditions are expressed in the form of curvilinear coordinates.

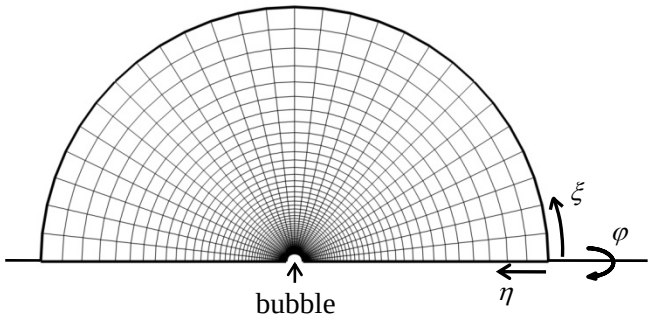

Figure 1. GRID AND COORDINATE SYSTEM

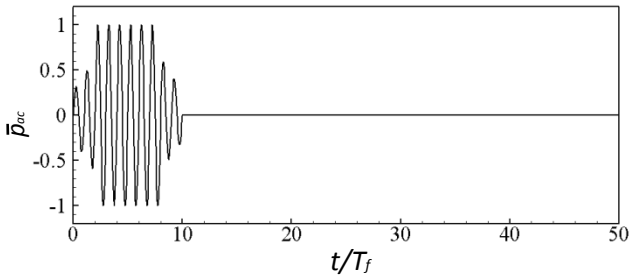

Figure 2. APPLIED ACOUSTIC PRESSURE.

Governing Equations

The flow field in the liquid is governed by the mass conservation and incompressible Navier-Stokes equations.

Equation of Continuity:

$$\frac{1}{h_\xi h_\eta \sigma}\Big[\frac{\partial}{\partial \xi}(h_\eta \sigma u_\xi)+\frac{\partial}{\partial \eta}(h_\xi \sigma u_\eta)\Big]=0. \tag{1}$$

Momentum Equation in ξ-direction:

$$\begin{aligned}&\rho\frac{\partial u_\xi}{\partial t}+\frac{\rho}{h_\xi h_\eta \sigma}\Big[\frac{\partial}{\partial \xi}(h_\eta \sigma u_\xi^2)+\frac{\partial}{\partial \eta}(h_\xi \sigma u_\xi u_\eta)\Big]\\ &=\frac{\mu}{h_\xi h_\eta \sigma}\Big[\frac{\partial}{\partial \xi}\Big(\frac{h_\eta \sigma}{h_\xi}\frac{\partial u_\xi}{\partial \xi}\Big)+\frac{\partial}{\partial \eta}\Big(\frac{h_\xi \sigma}{h_\eta}\frac{\partial u_\xi}{\partial \eta}\Big)\Big]\\ &\quad-\frac{1}{h_\xi}\frac{\partial p}{\partial \xi}+\frac{\rho}{h_\xi}\frac{\partial x}{\partial \xi}g+S_\xi,\end{aligned} \tag{2}$$

where S_ξ represents the apparent source term due to the changes in the basis vectors along ξ- and η-directions, i.e.,

$$\begin{aligned}S_\xi=&\frac{\rho u_\eta^2}{h_\xi h_\eta}\frac{\partial h_\eta}{\partial \xi}-\frac{\rho u_\xi u_\eta}{h_\xi h_\eta}\frac{\partial h_\xi}{\partial \eta}\\ &-\mu\frac{1}{\sigma^2 h_\xi}\frac{\partial \sigma}{\partial \xi}\Big(\frac{u_\xi}{h_\xi}\frac{\partial \sigma}{\partial \xi}+\frac{u_\eta}{h_\eta}\frac{\partial \sigma}{\partial \eta}\Big)\\ &+\frac{\mu}{h_\xi h_\eta \sigma}\Big[\frac{\partial}{\partial \xi}\Big(u_\eta\frac{\sigma}{h_\xi}\frac{\partial h_\xi}{\partial \eta}\Big)-\frac{\partial}{\partial \eta}\Big(u_\eta\frac{\sigma}{h_\eta}\frac{\partial h_\eta}{\partial \xi}\Big)\Big]\\ &+\mu\frac{1}{h_\xi h_\eta}\Big(\frac{\partial h_\xi}{\partial \eta}\frac{1}{h_\xi}\frac{\partial u_\eta}{\partial \xi}-\frac{\partial h_\eta}{\partial \xi}\frac{1}{h_\eta}\frac{\partial u_\eta}{\partial \eta}\Big)\\ &-\mu\frac{u_\xi}{h_\xi^2 h_\eta^2}\Big(\Big(\frac{\partial h_\xi}{\partial \eta}\Big)^2+\Big(\frac{\partial h_\eta}{\partial \xi}\Big)^2\Big).\end{aligned} \tag{3}$$

Momentum Equation in η-direction:

$$\begin{aligned}&\rho\frac{\partial u_\eta}{\partial t}+\frac{\rho}{h_\xi h_\eta \sigma}\Big[\frac{\partial}{\partial \xi}(h_\eta \sigma u_\xi u_\eta)+\frac{\partial}{\partial \eta}(h_\xi \sigma u_\eta^2)\Big]\\ &=\frac{\mu}{h_\xi h_\eta \sigma}\Big[\frac{\partial}{\partial \xi}\Big(\frac{h_\eta \sigma}{h_\xi}\frac{\partial u_\eta}{\partial \xi}\Big)+\frac{\partial}{\partial \eta}\Big(\frac{h_\xi \sigma}{h_\eta}\frac{\partial u_\eta}{\partial \eta}\Big)\Big]\\ &\quad-\frac{1}{h_\eta}\frac{\partial p}{\partial \eta}+\frac{\rho}{h_\eta}\frac{\partial x}{\partial \eta}g+S_\eta,\end{aligned} \tag{4}$$

where S_η is the one, in which ξ and η of Eqn. (3) are interchanged.

Boundary Conditions

On the far field: The transmit ultrasound is expressed by a pressure pulse on the far field consisting of a burst of 10 cycles, characterized by a dimensionless amplitude ε and driving frequency f. The first and last two cycles are modified by a Gaussian envelope. In Eqns. 5 and 6, p_{st} and p_{ac} are the ambient static pressure and the applied acoustic pressure, respectively. Fig. 2 shows the normalized applied acoustic pressure pulse $\bar{p}_{ac}$, that is, the shape of one pressure pulse.

$$p_\infty = p_{st}+p_{ac}, \tag{5}$$

$$p_{ac}=\bar{p}_{ac}\cdot \varepsilon p_{st}. \tag{6}$$

At the bubble surface: The normal and tangential force balances at the bubble surface are derived from the traction jump across the membrane, in which the viscous friction, surface tension at the gas-liquid interface and membrane tension (Eqns. 7 and 8) are considered. We assume the water and air system under the atmospheric pressure. The gas pressure p_g inside the bubble is considered as uniform distribution due to the sufficiently high speed of sound. The viscosity of the gas is negligibly smaller

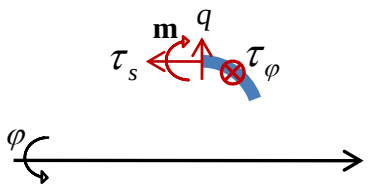

Figure 3. THE ELASTIC TENSIONS AND BENDING MOMENT DEVELOPING ON A PATCH OF MEMBRANE.

than that of the liquid. The normal stress balance is given by the modified Laplace's law

$$-p_l + 2\mu e_{\eta\eta} = -p_g + \gamma(\kappa_s + \kappa_\varphi) + F_n, \tag{7}$$

where F_n denotes the normal membrane traction. The shear stress balance is

$$2\mu e_{\eta\xi} = F_t, \tag{8}$$

where F_t denotes the tangential membrane traction. On the basis of the modelization in [21], F_n and F_t are written as the surface divergence of the elastic tension tensors on a patch of the membrane, i.e.,

$$F_n = \kappa_s\tau_s + \kappa_\varphi\tau_\varphi - \frac{1}{h_\xi\sigma}\frac{\partial}{\partial s}(\sigma q), \tag{9}$$

$$F_t = -\left[\frac{\partial\tau_s}{h_\xi\partial s} + \frac{1}{h_\xi\sigma}\frac{\partial\sigma}{\partial s}(\tau_s - \tau_\varphi) + \kappa_s q\right], \tag{10}$$

where τ_s and τ_φ are the principal in-plane tensions, and q the transverse shear tension (see Fig. 3), which is obtained from a torque balance in terms of the bending moments m_s and m_φ

$$q = \frac{1}{\sigma h_\xi}\frac{\partial\sigma}{\partial s}\left[\frac{\partial}{\partial\sigma}(\sigma m_s) - m_\varphi\right]. \tag{11}$$

Constitutive Laws

After establishing the force balance model, we proceed to specify the membrane material in order to relate the tensions of the membrane to its strains. Therefore, we should find some constitutive laws to approximate the physical behavior of a real material. One of the simplest constitutive models is the well-known Hooke law, which describes the linear relation between stress and strain. However, since the Hooke law assumes the infinitesimal displacement, its linearity restricts the reversibility in shape when the deformation is large. The hyperelastic materials, for which the surface energy function is defined as a function of the surface Green-Lagrange strain, are often employed to relate the finite deformation to the in-plane stress. There exist two common families, i.e., strain-hardening and strain-softening models. For strain-hardening material (e.g., red blood cell), the elastic modulus will rise as strain grows; in other words, the resonance frequency increases with the sound amplitude. The Skalak law [22] belongs to this kind of material. The strain-softening material (e.g., rubber) behaves in an opposite way to the strain-hardening material. One of the famous strain-softening models is the Mooney-Rivlin law. We use the neo-Hookean law, which is a special form of the Mooney-Rivlin law. The constitutive equations for the in-plane tensions are

$$\tau_s = \frac{G_s}{\lambda_s\lambda_\varphi}\left(\lambda_s^2 - \frac{1}{\lambda_s^2\lambda_\varphi^2}\right), \quad \tau_\varphi = \frac{G_s}{\lambda_s\lambda_\varphi}\left(\lambda_\varphi^2 - \frac{1}{\lambda_s^2\lambda_\varphi^2}\right), \tag{12}$$

where G_s is the surface shear elastic modulus, which characterizes the stiffness of the membrane. λ_s and λ_φ are the principal stretches respectively along the arc-length direction and along the azimuthal one, given by

$$\lambda_s = \frac{\mathrm{d}s}{\mathrm{d}s^R}, \quad \lambda_\varphi = \frac{\sigma}{\sigma^R}. \tag{13}$$

The constitutive equations for the bending moments are

$$m_s = \frac{E_b}{\lambda_\varphi}(K_s + \upsilon K_\varphi), \quad m_\varphi = \frac{E_b}{\lambda_s}(K_\varphi + \upsilon K_s), \tag{14}$$

where E_b is the bending modulus, which characterizes the bending resistance, and υ is the Poisson ratio, which is set to 0.5 indicating an incompressible material. K_s and K_φ are the surface bending strains given by

$$K_s = \lambda_s\kappa_s - \kappa_s^R, \quad K_\varphi = \lambda_\varphi\kappa_\varphi - \kappa_\varphi^R \tag{15}$$

RESULTS AND DISCUSSIONS

Both the results of gas microbubble and encapsulated microbubble are presented in this section. The shape oscillation of a gas bubble is compared with experimental and theoretical results to validate the numerical computation. Following that we will study the influence of membrane on the stability of the bubble surface and the effects of the amplitude of applied ultrasonic pressure.

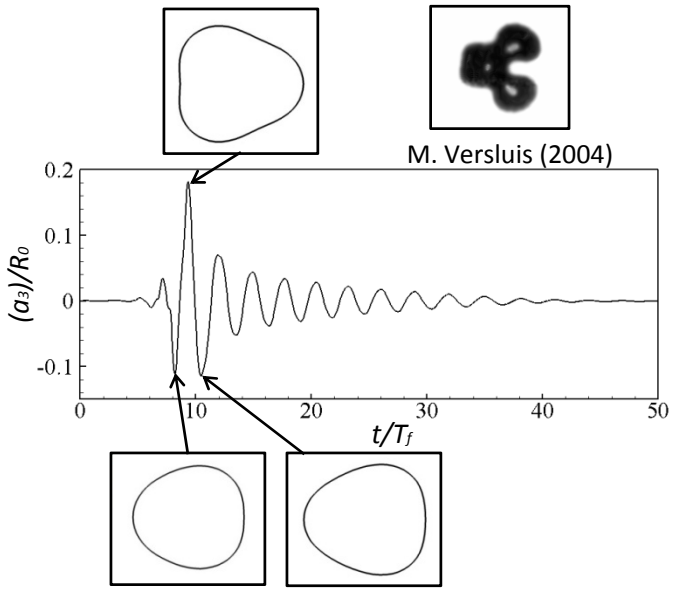

Figure 4. THE 3rd ORDER MODE OF GAS BUBBLE.

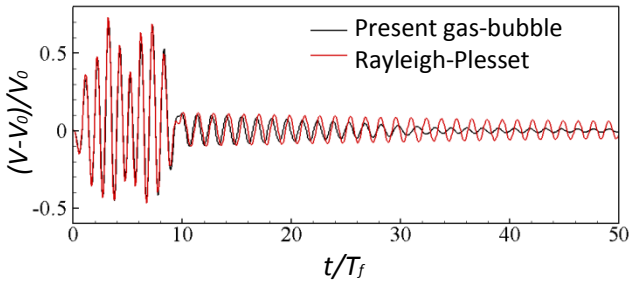

Figure 5. THE VOLUME RESPONSE OF GAS BUBBLE COMPARED WITH THE RAYLEIGH-PLESSET RESULTS.

Gas Bubble

We firstly consider a bubble without encapsulated membrane, which is called a gas bubble here, exposing in the ultrasound field. In this case, the bubble is purely subjected to surface tension, that is, the usual Laplace law ($F_n = 0$ in Eqn 7) and the free-slip condition ($F_t = 0$ in Eqn 8). In order to compare with the experimental and theoretical results of Versluis et al. [1], we set the bubble initial radius to 30μm, the frequency of driving acoustic pressure to 130kHz, and the amplitude to 0.4 of the ambient averaged pressure.

Expressing the bubble's shape in a spherical harmonics expansion form, we find that the third-order shape mode a_3 is preferentially unstable. The temporal evolution of the third-order mode a_3 normalized by the initial bubble radius R_0 is shown in Fig. 4. After several cycles of large-amplitude pulsations, the surface instability is excited for the higher-order modes. With the accumulation of parametric instability, the shape oscillation gets obvious. The surface modes are gradually damped due to the viscous effect after withdrawing the pressure pulse. Several snapshots of the computed bubble shape are presented in Fig. 4 with respect to the largest deformations. The preferred shape mode of a bubble with the specified radius and driving frequency is consistent with the experimental observation of Versluis et al. [1].

As shown in Fig. 5, the temporal change in the bubble volume is compared with the solution of the standard Rayleigh-Plesset equation which presents the radial motion of the spherical bubble. The beginning behavior of the present simulation before the shape oscillation gets obvious is in good agreement with the Rayleigh-Plesset solution. When the shape deformation becomes significant, the amplitude of our volume oscillation is smaller, and the damping is faster than in the Rayleigh-Plesset solution. This implies that the shape oscillation causes energy transfer from the purely radial oscillation, and thus more kinetic energy is consumed.

Encapsulated Bubble

In practical ultrasound contrast agents or drug delivery systems, the bubbles are encapsulated by membrane which is composed of albumin, galactose, lipid, or polymers. We here consider the hyperelastic membrane. The size of the encapsulated bubble is at the magnitude of micrometer allowing for safe medical application. Here we choose a bubble with equilibrium radius of $r_0 = 1\mu$m. For the membrane parameter, the surface shear modulus is set to $G_s = 0.03$N/m, and the bending modulus is set to $E_b = 2 \times 10^{-14}$N$\cdot$s.

As shown in Fig. 6, we firstly compare the volumetric variation of the bubble with and without membrane. A continuous pressure wave is imposed with a frequency of 1MHz and a dimensionless amplitude of 0.8. Under such a high frequency and large amplitude, the gas bubble presents higher harmonics when contracting (black line in Fig. 6). This is the famous Taylor instability happening at an interface between two fluids of different densities with the lighter fluid accelerating into the heavier fluid. The surface tension plays an important role on the stabilization in the radial motion for such a small bubble ($r_0 = 1\mu$m). Therefore, the emergence of the higher-order shape oscillation is suppressed so that the bubble keeps spherical all the time. When we add a membrane to the gas bubble, the amplitude is considerably attenuated. And the higher harmonics is further restrained. This indicates a more stable oscillation (blue line in Fig. 6). In reality, however, when a bubble is encapsulated with a membrane, the surface tension will be greatly reduced and can be negligible. Hence, we examined the case with membrane and zero surface tension. The volume of the encapsulated bubble (red line in Fig. 6) is larger than of the gas bubble when the bubble ex-

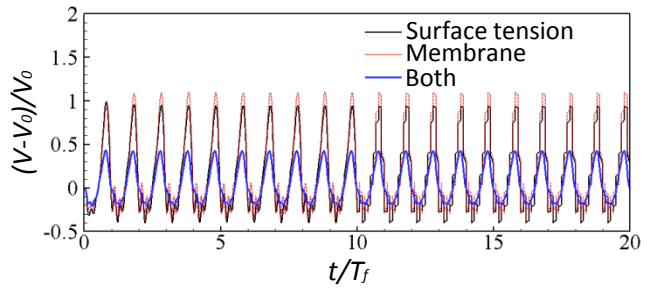

Figure 6. THE COMPARISON WITH AND WITHOUT MEMBRANE.

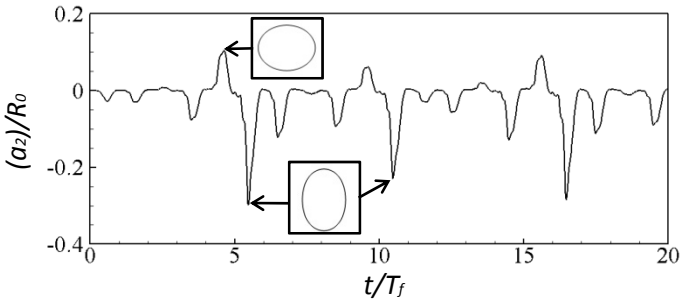

Figure 7. THE 2nd ORDER MODE OF ENCAPSULATED BUBBLE.

pands. The strain-softening characteristics involved in the constitutive law is reflected on this result. Further, when the bubble contracts, the higher harmonics are enhanced. In particular, a second-order shape mode emerges during oscillation in this condition (Fig. 7). The oblate and prolate shapes take place at the crest and trough, respectively. In addition, the oscillation of the second-order mode presents subharmonics characteristics, which is considered as a potential clinical application for ultrasonic imaging.

Finally, we investigate strain-softening characteristics of the membrane. The oscillatory amplitude of the bubble is increased through enhancing the acoustic pressure. We choose three pressure amplitude 0.1, 0.4 and 0.8, and compare the results with that from a modified version of Rayleigh-Plesset equation [23].

$$\ddot{r}+\frac{3}{2}(\dot{r})^2=\frac{1}{\rho}\Big[p_0\Big(\frac{r_0}{r}\Big)^3-p_\infty-\frac{4\mu}{r}\dot{r}-\frac{2\gamma}{r} -\frac{12G_s}{r_0}\Big(\frac{r-r_0}{r_0}\Big)\Big], \tag{16}$$

of which the last term inside the bracket in the right-hand-

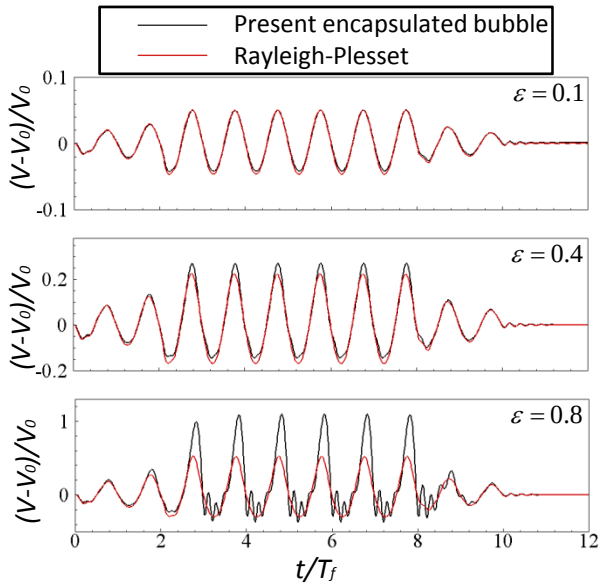

Figure 8. THE VOLUME RESPONSES OF ENCAPSULATED BUBBLE UNDER DIFFERENT ACOUSTIC PRESSURE.

side represents the normal stress based on the *linear* membrane model. Figure 8 shows the volume response of the encapsulated bubble for various acoustic amplitudes ε. For the smallest acoustic amplitude ($\varepsilon = 0.1$), the result based on the neo-Hookean model is in good agreement with that on the linear model, since both obey linearly perturbed oscillations. With the acoustic amplitude ε increasing, the neo-Hookean membrane bubble shows the enhanced symmetry breaking in the oscillation — larger expansion and smaller contraction — because of the augmented strain-softening effect. For the largest amplitude ($\varepsilon = 0.8$), the expansion approximates twice that of the linear model, and the higher harmonics appear during constriction as well.

CONCLUSIONS

We numerically investigated the dynamic behavior of encapsulated bubble in the ultrasound field. The mass conservation and Navier-Stokes equations were directly solved to obtain the flow field. The basic equations were discretized on a boundary fitted grid in order to accurately deal with the deformation of bubble. The dynamics of bubble surface was controlled by the traction jump equation coupling the membrane mechanics. In order to enclose the set of equations, we chose the neo-Hookean model as a constitutive law to describe the in-plane stress due to the finite surface deformation.

The numerical methods were firstly validated through computing the shape oscillation of a gas bubble driven by an applied pressure pulse. The results are qualitatively consistent with ex-

perimental and theoretical results [1]. Secondly, a bubble encapsulated by a neo-Hookean membrane was investigated. The nonlinear behavior of the membrane is presented referring to a linear model based on the Rayleigh-Plesset equation. With the increase of oscillatory amplitude, the membrane will experience a larger expansion and the higher harmonics when the bubble contracts. During this process, the second shape mode gets obvious and shows subharmonics characteristics.

ACKNOWLEDGMENT

The author Yunqiao Liu was supported through the Global COE Program, "Global Center of Excellence for Mechanical Systems Innovation," by the Ministry of Education, Culture, Sports, Science and Technology.

REFERENCES

[1] Versluis, M., van der Meer, S. M., Lohse, D., Palanchon, P., Goertz, D., Chin, C. T., de Jong, N. 2004, "Microbubble surface modes," *IEEE Ultrasounics Symposium*, 207–209.

[2] Lindner, J. R. 2004, "Microbubbles in medical imaging: current applications and future directions," *Nature Review Drug Discovery*, 3, 527–532.

[3] Allen, T. M., Cullis P. R. 2004, "Drug delivery systems: Entering the mainstream," *Science*, 303, 1818–1822.

[4] Plesset, M. S. 1954, "On the stability of fluid flows with spherical symmetry," *J. of Applied Physics*, 25, 96–98.

[5] Benjamin, T. B. 1964, "Surface effects in non-spherical motions of small cavities," *Cavitation in real liquids: proceedings of the Symposium on cavitation in real liquids, General Motors Research Laboratories*, Elsevier, New York, 164–180.

[6] Francescutto, A., Nabergoj, R. 1978, "Pulsation amplitude threshold for surface waves on oscillating bubbles," *Acoustica*, 41, 215–220.

[7] Yang, S. M., Feng, Z. C., Leal, L. G. 1993, "Nonlinear effects in the dynamics of shape and volume oscillations for a gas bubble in an external flow," *J. of Fluid Mechanics*, 247, 417–454.

[8] Feng, Z. C., Leal, L. G. 1993, "On energy transfer in resonant bubble oscillations," *Physics of Fluids A*, 5, 826–836.

[9] Mao, Y., Crum, L. A., Roy, R. A. 1995, "Nonlinear coupling between the surface and volume modes of an oscillating bubble," *J. of the Acoustical Society of America*, 98, 2764–2771.

[10] McDougald, N. K., Leal, L. G. 1999, "Numerical study of the oscillations of a non-spherical bubble in an inviscid, incompressible liquid. Part I: free oscillations from non-equilibrium initial conditions," *Int. J. of Multiphase Flow*, 25, 887–919.

[11] McDougald, N. K., Leal, L. G. 1999, "Numerical study of the oscillations of a non-spherical bubble in an inviscid, incompressible liquid. Part II: the response to an impulsive decrease in pressure," *Int. J. of Multiphase Flow*, 25, 921–941.

[12] Chomas, J. E., Cayton, P. A., May, D., Allen, J., Klibanov, A., Ferrara, K. 2000, "Optical observation of contrast agent destruction," *Applied Physics Letters*, 77, 1056–1058.

[13] Bloch, S. H., Wan M., Dayton P. A., Ferrara, K. W. 2004, "Optical observation of lipid- and polymer-shelled ultrasound microbubble contrast agents," *Applied Physics Letters*, 84, 631–633.

[14] de Jong, N., Cornet, R., Lancée, C. T. 1994, "High harmonics of vibrating gas-filled microspheres. Part one: simulations," *Ultrasonics*, 32, 447–453.

[15] Church, C. C. 1995, "The effects of an elastic solid surface layer on the radial pulsations of gas bubbles," *J. of the Acoustical Society of America*, 97, 1510–1521.

[16] Holzapfel, G. A. 2000, *Nonlinear Solid Mechanics,* John Wiley & Sons Ltd, England.

[17] Barthès-Biesel, D., Diaz, A., Dhenin, E. 2002, "Effect of constitutive laws for two-dimensional membranes on flow-induced capsule deformation," *J. of Fluid Mechanics*, 460, 211–222.

[18] Tsiglifis, D., Pelekasis, N. A. 2007, "Nonlinear radial oscillations of encapsulated microbubbles subject to ultrasound: The effect of membrane constitutive law," *J. of the Acoustical Society of America*, 123, 4059–4070.

[19] Takagi, S., Prosperetti, A., Matsumoto, Y. 1994, "Drag coefficient of a gas bubble in an axisymmetric shear flow," *Phys. Fluids*, 6, 3186–3188.

[20] Takagi, S., Matsumoto, Y., Huang, H. 1997, "Numerical analysis of a single rising bubble using boundary-fitted coordinate system," *JSME Int. J.*, B40, 42–50.

[21] Pozrikidis, C., 2003, *Modeling and Simulation of Capsules and Biological Cells*, Chapman & Hall/CRC, London.

[22] Skalak, R., Tozeren, A., Zarda, R. P., Chien, S. 1973, "Strain energy function of red blood cell membranes," *Biophysical J.*, 13, 245–264.

[23] Hoff, L. 2001, *Acoustic Characterization of Contrast Agents for Medical Ultrasound Imaging*, Kluwer Academic Publishers, Netherlands.